Energy xxx (2016) 1–16

Contents lists available at ScienceDirect

Energy

journal homepage: www.elsevier.com/locate/energy

Analysis and comparison of solar-heat driven Stirling, Brayton and Rankine cycles for space power generation

Claudia Toro [a, *], Noam Lior [b]

[a] Department of Mechanical and Aerospace Engineering, University of Rome "Sapienza", Rome, Italy
[b] Department of Mechanical Engineering and Applied Mechanics, University of Pennsylvania, Philadelphia, PA, USA

ARTICLE INFO

Article history:
Received 11 May 2016
Received in revised form
4 November 2016
Accepted 18 November 2016
Available online xxx

Keywords:
Space power generation
Space thermal power
Space dynamic power
Thermal cycle
Brayton cycles
Rankine cycles
Stirling cycles

ABSTRACT

This paper presents an analysis of solar-heat driven Brayton, Rankine and Stirling cycles operating in space with different working fluids. Generation of power in space for terrestrial use can represent a great future opportunity: the low-temperature of space (~3 K), allows the attainment of very high efficiency even with low-temperature heat inputs, and the solar energy input is higher in space than on earth. This paper shows a comparative analysis of advanced Brayton, Rankine and Stirling cycles to improve the understanding of the optimal trade-off between high efficiency and the smallest needed heat rejection area. The effect of the main cycles' operational parameters and plant layouts on efficiency and power to radiator area ratio have been analyzed. The thermal efficiency of regenerative-reheated-intercooled Brayton cycle was found to be the best among the investigated configurations. The power to radiator area ratio was found to increase with the introduction of reheating for both the Rankine and Brayton cycles. Stirling cycles efficiencies are lower than those obtained by the Brayton and Rankine cycles but with values of power to radiator area ratio equal to about half of those obtained by Brayton cycles but much higher than those obtained by the Rankine cycles.

1. Introduction

As published over the past few decades [1–5], generation of power in space offers a promising opportunity for both space missions and terrestrial use. Rapidly escalating problems of energy, environment and increased and more demanding population make it increasingly difficult to generate power, heat, light and food on earth [6]. As described in the publications by Glaser and co-workers (e.g., [7,8]), Mankins [1,9], Criswell and co-workers [9], Brown [10], Woodcock [11], Lior and co-workers [2,12,13] and many others, space has many desirable attributes for serving as the location for supplying energy to earth by constructing space satellites (SPS—solar power satellite) or moon-based power generation stations where the power is beamed to earth by microwave or laser for use. Three of the key advantages are a significant reduction in greenhouse gas and other emissions, reduction in the need for terrestrially-based power generation plants and thus of their undesirable environmental and social impacts, and effective use of solar energy. This topic has received significant support by the U.S. NASA during the late 1970s till the early 1990s, and beginning somewhat later is to some extent still continuing by several European countries and Japan, and recently in China. It is interesting that California Pacific Gas & Electric, a major U.S. electricity and gas utility, signed a contract with Solaren Corporation to furnish, in 2016, 200 MW (megawatt), enough for a small city's needs, microwave beamed from geosynchronous (stationary) earth orbit (GEO) to a rectenna in the city Fresno, California.

To be considered as a viable alternative, a space power generation system must be very lightweight to reduce launch costs (they form the largest part of the generated electricity cost), be extremely reliable and long-lived to minimize maintenance and upkeep requirements, and for terrestrial use provide very high power levels to the transmission beam power source to maximize the delivered power to Earth [4]. Most such systems use solar photovoltaic electricity generators, but solar heat power systems ("Dynamic Systems", DS) are considered in many studies (e.g., [3–15]) to be a more viable alternative.

In particular, thermal power systems using space as a low temperature (~3 K) heat sink are theoretically able to produce continuous (or near-continuous, depending on the orbit) power at a very high efficiency compared with terrestrial ones. In these closed

* Corresponding author.
E-mail address: claudia.toro@uniroma1.it (C. Toro).

http://dx.doi.org/10.1016/j.energy.2016.11.104
0360-5442/

loop "Dynamic Systems", heat could be generated by a solar or nuclear source and rejected to space by a radiator, and the output power is generated by a turbine or perhaps a Stirling-type engine.

An important issue in the design and subsequent possible commercialization of such "Dynamic Systems" is related to the choice of the working fluid, which affects not only the thermal efficiency but also the overall weight of the system. The reduction of the total weight of the system is in fact one of the main objectives in the design of these cycles because it is directly related to the costs of transporting them to space, which is currently the dominant fraction of the total cost [14]. The radiator is the largest component of a space nuclear dynamic systems and one of the largest components in solar dynamic systems [15,16] (the second in size is the solar collector) and it is a major weight contributor in both systems [17]. For these reasons the thermodynamic analysis of these cycles should be coupled with the radiator heat exchange calculation to find the best tradeoff between system efficiency and power-to-weight ratio.

Promising options for space thermal power plants include Brayton, Ericsson, Rankine and Stirling cycles [4,5,12].

Rankine systems have the distinct efficiency advantage because their backwork ratio is very small when compared with all-gas systems [9], and the high efficiency reduces the needed radiator area and weight. Much attention has been given by researchers to the Rankine system using liquid metal working fluid, which also has the advantage of high heat transfer coefficients in the solar collector and the heat rejection radiator [18]. In space thermal systems, for similar turbine inlet temperatures a Brayton cycle radiator may require more than ten times the specific area required for a liquid metal Rankine cycle radiator. However the Brayton cycle merits consideration because its use eliminates problems associated with two phase flow in a zero gravity environment and with the presence of corrosive working fluid and the related possibility of corrosion and/or erosion damage to the rotating components [17].

The Brayton cycles are a mature technology and were considered as the most promising power generation system for near future application of the space station [14]. Much of the required equipment and technology for the Brayton cycle is available and this system has a good potential for multiple starts as well as for achieving required long time reliability.

Space Brayton technology has been under development for over 40 years. In the 1960's, several 10 kW Brayton Rotating Units (BRU) were designed, developed and tested [19]. Much of the development experience from the BRU units went into the design of a 25 kW DS module for Space Station Freedom during the 1980's. Under the Freedom program, detailed designs for the solar concentrator, heat receiver and radiator were completed [15]. In this project the gaseous working fluid for the regenerated Brayton cycle is a mixture of helium and xenon with an equivalent molecular weight of 40, which was stated to result in the best combination of heat transfer and thermodynamic performance. With a turbine inlet temperature of about 1,000 K (selected so that refractory materials are not needed anywhere in the system), the NASA dynamic system had a thermal efficiency of about 33%.

A subscale of the Freedom module was proposed for a fully integrated system ground test [20] in a simulated space environment. The main test objectives were to demonstrate DS system capability to produce power in the simulated space environment, to determine the overall system efficiency and compare it to competing technology, and to identify main technical issues. The system has accumulated nearly 800 h of operation and the DS efficiency (ratio of electrical energy output to solar energy collected, over a period of an orbit) have been measured to be up to 17% [21].

These tests allowed to identify a number of technical issues concerning dynamic power systems including the use of gas bearings, hermetic sealing of the power conversion unit, potential vibration concerns and system mass limitations, and the program was later cancelled.

In the early 2000's NASA [22] began the Nuclear Systems Initiative which led to the Prometheus Program and the Jupiter Icy Moons Orbiter (JIMO) mission. The JIMO design studies considered liquid-metal cooled, gas cooled, and heat pipe cooled reactors as well as Brayton, Stirling, and thermoelectric power conversion. Although the JIMO Project was terminated by NASA in 2005, some technology development was completed on Brayton. The 2-kWe Brayton Power Conversion Unit (BPCU) from the SD GTD was modified with an electrical heat source and utilized in a number of demonstration tests. The activities conducted during JIMO related to Brayton technology included high power alternator testing, gas foil bearing testing, and superalloy material testing.

As highlighted in Ref. [4], advanced DS have long term potential to reach specific power generation rates of over 700 W/kg with a system specific encumbrance area of 450 W/m^2.

The performance of different types of dynamic systems were also evaluated by some researchers [12,17] as a function of the type of working fluid, for simple or regenerated cycle configurations.

Glassman and Stewart [17] focused on the evaluation of the effect of some cycles temperature ratio (turbine exit to inlet, compressor exit to inlet, and compressor inlet to turbine inlet) on thermal efficiency and radiator area of an ideal gas regenerated Brayton cycle. Regenerated Rankine, Brayton and Ericsson cycles were evaluated by Tarlecki et al. [12] for different working fluids, in particular argon (Ar), nitrogen (N_2), argon-xenon (Ar-Xe, 50% Ar by weight), helium (He), helium-xenon (He-Xe, 50% He by weight) and hydrogen (H_2) for Brayton and Ericsson, and only the first two for the Rankine cycle. The results obtained highlight the higher theoretical thermal efficiency achievable with diatomic gases (H_2 and N_2) in both Brayton (63%) and Rankine cycles (85%). They also found that although the Rankine cycles have a higher thermal efficiency, they require a much larger radiator area due to their lower condensation temperatures.

Massardo et al. [23,24] have shown that the performances of DS can be improved by utilizing combined (Solar Dynamic Combined Cycle - SDCC) or binary cycle concepts. They studied the possibility of recovering a fraction of the heat rejected from a closed Brayton cycle (CBC) system (He-Xe) by an organic Rankine cycle bottoming system. Several different fluids have been considered, but only R22, R114 and Toluene were considered to be well suited to the temperature values in the ORC subsystems. These fluids allow operation at supercritical cycle conditions (thus minimizing two-phase flow regimes); Using R22 and R114, the ORC system can operate in the range of 0–200 °C; when using Toluene the temperatures must be higher to attain supercritical conditions. Besides, since toluene has very low condensation pressure at low temperatures (<30 °C), it is necessary to use higher radiator temperatures. Thus, in this case, the minimum allowable radiator temperature is about 60–70 °C. The efficiency increase is generally equal to 4% but the reduction of the SDCC specific parameters (area and mass) is too small to justify the use of the more complicated SDCC system as compared with a simpler CBC one.

They also evaluated a Solar Dynamic Binary Cycle (SDBC). This power system is composed of two Rankine cycles: the topper is a Mercury Rankine Cycle (MRC) and the bottomer is an organic Rankine cycle. They show that efficiencies are above 40% in all ranges of analyzed mercury maximum temperature, and performance improvements take place in efficiency, weight, and heat transfer area, and thus these claimed advantages of SDBC over CBC were considered to justify the use of the more complicated SDBC system.

Please cite this article in press as: Toro C, Lior N, Analysis and comparison of solar-heat driven Stirling, Brayton and Rankine cycles for space power generation, Energy (2016), http://dx.doi.org/10.1016/j.energy.2016.11.104

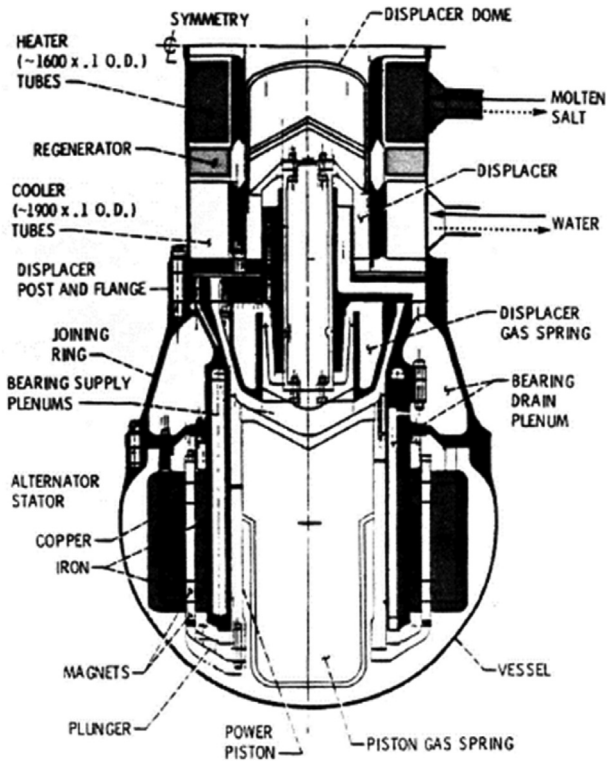

Fig. 1. 25 kW Stirling engine developed under the SSP100 program [25].

The Stirling free-piston engine [5,25,26] has many attractive attributes for space power applications. The Stirling cycle is probably the most efficient existing heat engine cycle and in the free-piston configuration (FPSE) it also has a long-life potential because it uses gas bearings and has a relative simple setup with only two moving parts per cylinder (the displacer and the power piston/alternator plunger). FPSE have the potential of meeting future space power requirements of high reliability, long life, and efficient operation for a wide variety of applications with less mass, better efficiency, and less total heat exchanger area (collector and radiator) than other power converter options [25]. FPSEs can be coupled with many potential heat sources (solar, radioisotope, or nuclear reactor), various heat input systems (direct radiation or conduction, heat pipe, or pumped loop), various heat rejection systems (heat pipe or pumped). The NASA Stirling Space Engine Program (SSP) [27], performed between 1988 and 1993, had the main objective to develop the technology necessary for operating Stirling power converters in a space environment and to define and build a Reference Space Stirling Power Converter (RSSPC). The program concluded before the construction of the SSPC due to the termination of program funding.

The design goals established for the RSSPC were an output power up to 25 kWe per cylinder, with an efficiency of 25% (electrical power out/heat into heater head) and heater wall temperature and cooler wall temperature of 1050 K and 525 K, respectively, and a target specific mass of 6 kg/kW or less for a design life of 60,000 h of unattended operation with the power module capable of sustaining at least 200 start-stop cycles. The final design configuration selected for the RSSPC was a stepped-bore arrangement with the displacer and power piston supported on internally pumped hydrostatic gas bearings. Fig. 1 is a cross section of half of the 25 kW engine developed under the SSP program. To minimize the power module specific weight, the working fluid pressure and the operating frequency needed to be made as high as possible. The RSSPC uses helium at 150-bar mean pressure as the working fluid. There is a recently renewed interest in free-piston Stirling engine converters for use in space power applications [26,28]. Under 2001 NASA SBIR Phase I funding, Sunpower optimized and designed a small FPSE converter with a reject temperature of 393 K and an 83% efficient alternator producing 33 W for 115 W of heat input, and with a mass of only 305 g. In Ref. [26] gas-cooled Brayton, liquid metal Stirling, and liquid-metal thermoelectric mass and performance estimates have been analyzed for 50 kWe class lunar and Mars surface power applications with scaling from 25 to 200 kWe. The analyses indicate that among the 50 kWe stainless steel reactor options, the liquid-metal Stirling system provides the lowest mass at about 5300 kg followed by the gas-cooled Brayton at 5700 kg, and the liquid-metal thermoelectric (direct energy conversion) at 8400 kg.

The present study that represents an in-depth, extended development of [29] aims to investigate complex and promising Brayton and Rankine cycle configurations, using the working fluids identified as the best performing in the previous study and also analyze and compare the performance of a free-piston Stirling engine cycle. A comparative analysis of Brayton, Rankine and Stirling power cycles operating in space with different layouts and working fluids has been performed. Specifically for the Brayton, H_2 and N_2 and their mixtures have been considered, for the Rankine, N_2 and Ar, and for the Stirling H_2, N_2 and He.

Table 1
Major properties of the considered working fluids.

Working fluid	Operating conditions	Ar	H_2	N_2	50%$_{vol}$ H_2/50%$_{vol}$ N_2	50%$_{vol}$Ar/50%$_{vol}$$N_2$	50%$_{vol}$ Ar/50%$_{vol}$ H_2
Condensation temperature, [K]	p = 1 bar	87	20.2	77.1	71.6	83.1	80.9
Specific heat, c_p [kJ/kgK]	p = 1 bar T = 200 K	0.52	14.03	1.044	1.91	0.55	1.16
	p = 10 bar T = 1500 K	0.52	16.03	1.24	2.23	0.57	1.26
Speed of sound, c [m/s]	p = 1 bar T = 200 K	263	1081	288	394	264	346
	p = 10 bar T = 1500 K	721	2886	764	1050	717	930
Density, ρ [kg/m^3]	p = 1 bar T = 200 K	2.40	0.12	1.68	0.90	2.32	1.26
	p = 10 bar T = 1500 K	3.20	0.16	2.24	1.20	3.10	1.68
Thermal conductivity, $k \times 10^6$ [kW/m K]	p = 1 bar T = 200 K	12	127	18	58	13	51
	p = 10 bar T = 1500 K	52	540	82	254	55	213

Please cite this article in press as: Toro C, Lior N, Analysis and comparison of solar-heat driven Stirling, Brayton and Rankine cycles for space power generation, Energy (2016), http://dx.doi.org/10.1016/j.energy.2016.11.104

Table 2
Relative Stirling performance of selected working fluid.

Gas	Specific heat, c_p [kJ/kgK]	Density, ρ [kg/m^3]	Thermal conductivity, k [W/mK]	Q_{wf}	C
H_2	14.54	0.042	0.27	2.32	0.44
N_2	1.07	0.58	0.039	0.644	0.06
He	5.19	0.0832	0.241	0.984	0.55
Ar	0.52	0.83	0.028	0.311	0.06
CO_2	1.06	0.914	0.034	1	0.03

The study started by repeating with the Camel software [30] the simulations of the basic system configurations analyzed in Ref. [9] that were originally performed by using Aspen Plus software, just to validate the method and then continued with the main contribution in this paper, which is a successive analysis of different system configurations that add reheating, intercooling, and both.

As in Ref. [12], three primary performance criteria were used for evaluating and comparing the different cycles and working fluids: the energy efficiency η_I, the exergy efficiency ε, and the ratio of the power output to required radiator area, Ψ [kW/m^2], which are defined, respectively, as:

$$\eta_I = \frac{W}{Q_{in}} \tag{1}$$

$$\varepsilon = \frac{W}{(Ex_{out} - Ex_{in})_{heat\ \ addition}} \tag{2}$$

$$\psi = \frac{W}{A_{rad}}, \tag{3}$$

where W is the output power, Q_{in} is the input heat flux, Ex_{in} and Ex_{out} are inlet and outlet exergy in the heat addition process, and A_{rad} is the radiator area.

The analysis presented here was developed throughout the use of an in-house process simulator CAMEL-Pro™ [31]. It is written in C#, based on an object-oriented approach, and equipped with a user-friendly graphical interface, the CAMEL-Pro™ Simulator, that allows for the simulation and analysis of several energy conversion processes [32,33]. The system is represented as a network of components connected by material and energy streams; each component is characterized by its own (local) set of equations describing the thermodynamic changes imposed on the streams. A big advantage of CAMEL-Pro™ is its modularity that enables users to expand the code by adding new components or by modifying the model of the existing ones: we used these capabilities to introduce the proper process equations, in particular we modified existing components introducing new specific configurations for the selected working fluids. It is equipped with several libraries of thermodynamic properties for the calculation of thermodynamic and transport properties of fluids [34]. The properties of the fluids considered in this study at the space temperature and pressures were calculated by the RefProp Database (Reference Fluid Thermodynamic and Transport Properties Database) [35] library.

2. Selection of working fluids and reference environment

2.1. The reference space environment

As briefly introduced above, the space environment represent the space-based thermal power generation system heat sink and therefore becomes crucial to set proper values for the temperature and pressure that are, in turn, both fundamental to evaluate the system thermodynamic performance, to design the heat rejection radiator and set the dead state for the exergy analysis.

The temperature of space (due to the cosmic background radiation) is generally agreed to be about 3 K and is assumed here to be the lowest that space can offer and is thus useful for estimating the maximal thermodynamic potential of space and consequently used as the above-mentioned dead state temperature. The actual temperature in space depends also strongly on the effect of the radiation from the sun, the earth and other surrounding planets, and other stars, which continuously change with time, most immediately due to their ongoing motion. For example, the sunlit side of objects in space at Earth's distance from the Sun can climb to over 393 K, and the shaded side to lower than 173 K. These temperatures drop steeply with the distance from earth.

The pressure environment is complex and may be significantly non-uniform, in large part due to the motion of the space vehicle. At a height of 320 km (in Low Earth Orbit, LEO) from the Earth surface, an orbiting object can be in a pressure field varying between 10^{-8} bar in the front to 10^{-10} bar in the rear due to collisions with the ambient rarefied atmosphere. Assuming an orbital velocity of about 8 km/s, the dead state pressure (p_0) was selected to be 10^{-8} bar [14].

2.2. The working fluids

The working fluids chosen to develop this work are H_2 and N_2 and their mixtures for the Brayton cycle, Ar and N_2 and their mixtures for the Rankine cycle [12,36] and H_2, N_2 and He for the Stirling cycle.

The main properties of the listed fluids under the conditions of our interest are shown in Table 1.

The Carnot efficiency equation

$$\eta_I = 1 - \frac{\overline{T}_L}{\overline{T}_H}, \tag{4}$$

where T_H and T_L are the cycle average heat input and rejection temperatures, respectively, shows that this thermal efficiency rises as T_L is decreased. Space based systems have in that way a significant advantage since their temperature of about 3 K makes it possible to reach cycle heat sink temperatures (T_L) much lower than in terrestrial systems, which allows attainment of high power system efficiencies that are also almost independent of the heat input temperature. For Brayton and Stirling cycles that use a gaseous working fluid throughout, it is advantageous to exploit the fluids that are characterized by the lowest condensation temperatures at the cycle low pressure, because that allows operation at the lowest possible sink temperature. Condensing those gases at very low temperatures would theoretically favor the Rankine cycle as it allows much higher efficiency due to its much smaller backwork ratio. Furthermore, in the Rankine cycle the working fluid should have a low triple point temperature and pressure to take advantage of the low heat sink temperature and widen the possible working area of the fluid.

For Brayton and Rankine cycles, following the analysis performed in Ref. [12], two properties have a major effect on the

Please cite this article in press as: Toro C, Lior N, Analysis and comparison of solar-heat driven Stirling, Brayton and Rankine cycles for space power generation, Energy (2016), http://dx.doi.org/10.1016/j.energy.2016.11.104

system performance: c_p and $(1-c_v/c_p)$, and we thus use them to also choose the working fluids that are best for this kind of applications. Increasing c_p raises both cycle efficiency and heat transfer rates and it is thus better to use fluids with a higher value of c_p. As shown in Table 1, the high value related to H_2 made it the most useful from that standpoint. Argon on the other hand shows a relatively low c_p even in mixtures with H_2 or N_2.

The term $(1-c_v/c_p)$, becomes relevant during the expansion and compression processes in the power cycles, representing the exponent of the isentropic relation

$$T_{out} = T_{in}\left(\frac{p_{out}}{p_{in}}\right)^{1-\frac{c_v}{c_p}} \tag{5}$$

Dealing with regenerative cycles, once the pressure ratio is fixed smaller $(1-c_v/c_p)$ are preferable allowing to increase the turbine exit temperature and thus also the amount of heat available for regeneration.

As reported in Ref. [12], Argon has, in that sense, the worst value of $(1-c_v/c_p)$ among the fluids we investigated, and pure N_2 and H_2 are the best.

The flow situation in a Stirling engine is more complex, making the comparison of the effects of different working fluids on system efficiency more difficult. Transport properties, such as viscosity, thermal conductivity, specific heat, and density, affect heat transfer and aerodynamic friction losses. c_p and k are parameters which principally control heat transfer to and from the cooler, heater and regenerator. ρ and μ affect friction losses which control the pump work. The working fluid in a Stirling engine should have high thermal conductivity, high specific heat capacity and low viscosity. Martini [37] and Clarke [38] defined the efficacy of a working fluid for the Stirling cycle in terms of specific heat capacity, thermal conductivity and density, which is useful for preliminary selection of working fluids, as:

$$C = \frac{k}{c_p \cdot \rho} \tag{6}$$

The Stirling analysis approach proposed by Walker [39] is to consider a steady flow situation where both good heat transfer and low pumping losses are taken assumed. For these reasons exploiting the Reynold's analogy as in Ref. [39], in a given situation with specified temperatures and pumping power to heat transfer (P/Q) ratio, it is possible to use the relation [29]:

$$Q_{wf} \propto \left(\rho^2 c_p^3\right)^{0.5} \tag{7}$$

as a useful measure for comparing the relative merits of working fluids for Stirling engines.

Table 2 shows the comparison of various fluids when using Eqs. (6) and (7) at the average temperature and pressure of 600 K and 1 bar. It may be seen that none of these working fluids satisfies these two requirements at the same time. E.g., comparing the values of Q_{wf}, hydrogen is the preferred heat transfer fluid, with helium and carbon dioxide a second choice, while comparing the capacity factor C, the best one is He followed by H_2.

Consequently, three different working fluids, H_2, N_2 and He, are considered in this study for the Stirling Engine, while N_2 and H_2 are used as heat exchange working fluids in both the cold and hot sides of Stirling cycles for a direct comparison with the simulated Brayton and Rankine cycles.

Expanding eq. (3) that defines the radiator required area parameter,ψ,

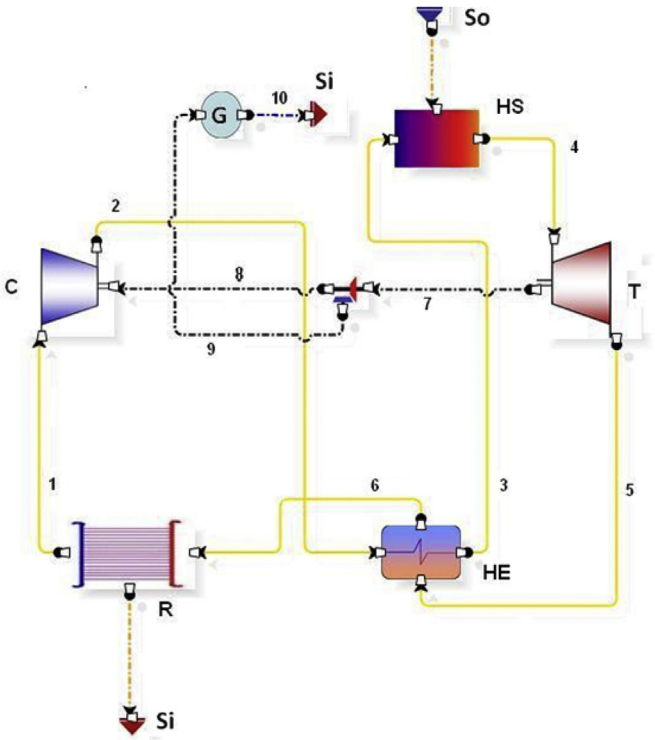

Fig. 2. Layout of the simulated regenerative Brayton cycle (R-B) in CAMEL-Pro™ C-Compressor; T-Turbine; HE- Heat Exchanger; R- Radiator; HS-Heat Source; G-Generator; So-Source; Si-Sink; —: *Working Fluid*; -•-•-•-: *Power (shaft, electric and heat).*

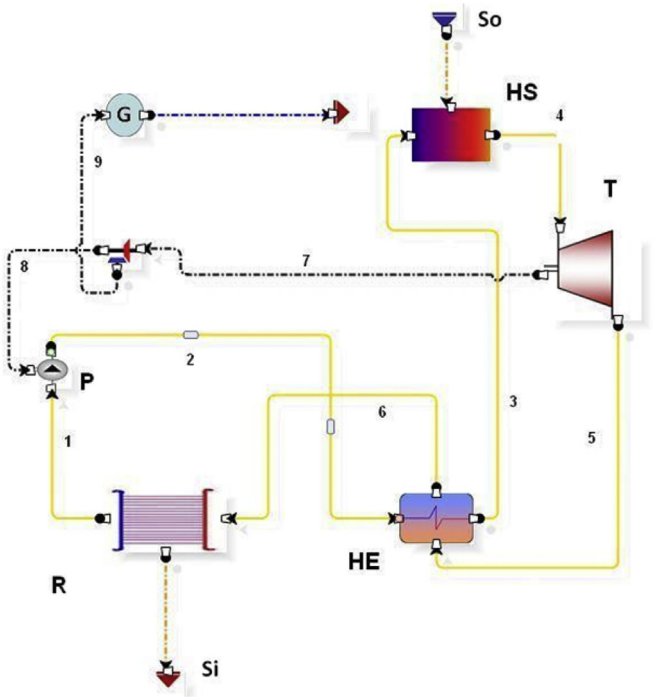

Fig. 3. Layout of the simulated regenerative Rankine cycle (R-R). P-Pump; T-Turbine; HE- Heat Exchanger; R- Radiator; HS-Heat Source; G—Generator; So-Source; Si-Sink; —: Working Fluid; -•-•-•-•: Power (shaft, electric and heat.

Please cite this article in press as: Toro C, Lior N, Analysis and comparison of solar-heat driven Stirling, Brayton and Rankine cycles for space power generation, Energy (2016), http://dx.doi.org/10.1016/j.energy.2016.11.104

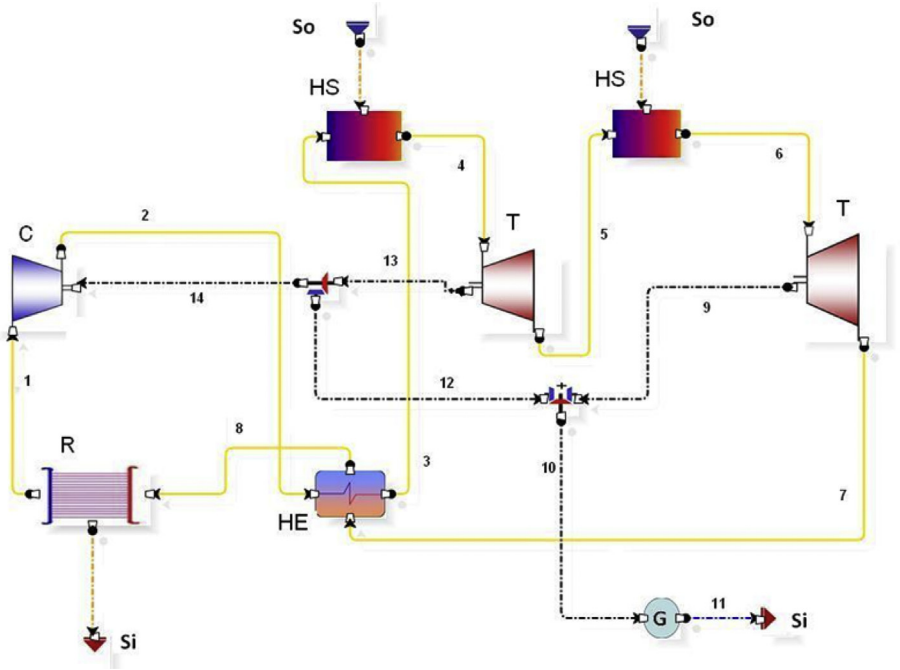

Fig. 4. Layout of the simulated regenerative-reheated Brayton cycle (R-R-B). C-Compressor; T-Turbine; HE- Heat Exchanger; R- Radiator; HS-Heat Source; G-Generator: So-Source; Si-Sink; —: *Working Fluid*; -•-•-•-•: *Power (shaft, electric and heat).*

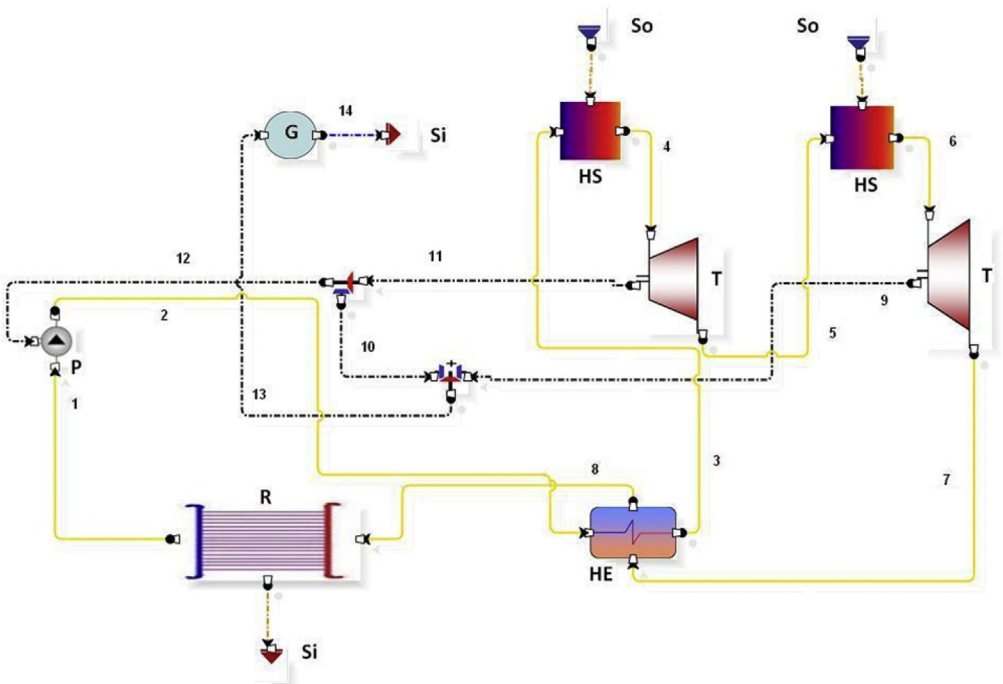

Fig. 5. Layout of the simulated regenerative – reheated Rankine cycle (R-R-R). P-Pump; T-Turbine; HE- Heat Exchanger; R- Radiator; HS-Heat Source; G—Generator; So-Source; Si-Sink; —: *Working Fluid*; -•-•-•-•-: *Power (shaft, electric and heat).*

$$\psi = \frac{W}{A_{rad}} = \frac{W}{Q_{out}/U_{rad}} = \frac{W}{(Q_{in} - W)/U_{rad}} = \frac{W}{W[(1/\eta_I) - 1]/U_{rad}} = \frac{U_{rad}}{[(1/\eta_I) - 1]} \quad (8)$$

shows that ψ would rise with the cycle energy efficiency η (because more efficient cycles reject less heat) and with the overall heat transfer coefficient of the radiator, U_{rad}. The working fluids thus affect ψ both in their effect on the cycle efficiency, η_I, and in their effect on U_{rad}.

Please cite this article in press as: Toro C, Lior N, Analysis and comparison of solar-heat driven Stirling, Brayton and Rankine cycles for space power generation, Energy (2016), http://dx.doi.org/10.1016/j.energy.2016.11.104

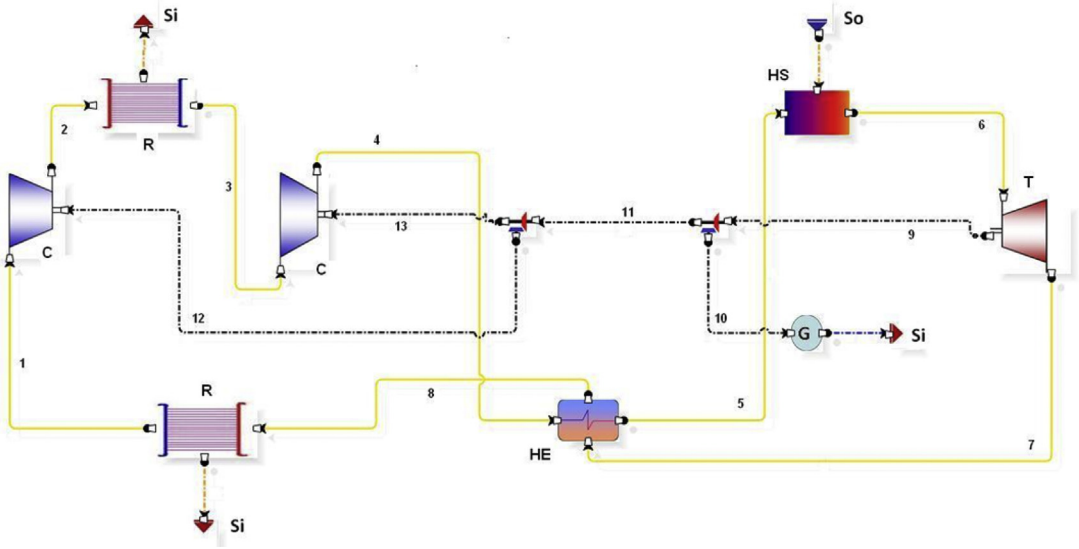

Fig. 6. Layout of the simulated regenerative-intercooled Brayton cycle (R-I-B). C-Compressor; T-Turbine; HE- Heat Exchanger; R- Radiator; HS-Heat Source; G-Generator; So-Source; Si-Sink; —: *Working Fluid*; -·-·-·-·-: *Power (shaft, electric and heat).*

3. Cycle configurations

The layouts of the systems analyzed in this study are shown in Figs. 2–7.

The first step of this analysis has been the validation of the implemented model by comparison of our simulation results for the regenerative Rankine (Fig. 2) and Brayton (Fig. 3) cycles with the simulations results from Ref. [12].

The assumption to fix the p_L and T_L of the Rankine cycle at 0.75 bar and 84 K for Ar, and 0.15 bar and 64 K for N_2, derives from the necessity of exploiting the maximum pressure and temperature drop up to the limit of the triple point (Ar: T_{tp} = 83.8 K, p_{tp} = 0.69 bar; N_2: T_{tp} = 63.15 K, p_{tp} = 0.13 bar).

The turbine inlet temperature (TIT) selected was 1500 K, which is well within the values of terrestrial gas turbine power plants (for example, the Mitsubishi Heavy Industries gas-turbine system reaches a TIT of 1773 K [40]). The present analysis focuses on high power systems that use axial flow turbines, which typically easily allow the use of blade cooling, in consideration of the fact that state of the art Turbine blade cooling includes several methodologies and that the specific peculiar space environment where the Turbine object of the present study operates might strongly affect the improvement in the cooling efficiency and furthermore, given that modern engines bled off for cooling and sealing purposes for nozzle guide vanes and turbine blades around 20% of the compressed air, we assumed that neglecting the impact of the cooling system might not affect so much the performance evaluation. The use of N_2 and Ar at such temperatures has been proven to be suitable in other studies [41].

The results obtained with our CAMEL-Pro process simulator for the same operative conditions of [12] are shown in Table 3 alongside those of [12], and are in excellent agreement, within 3%.

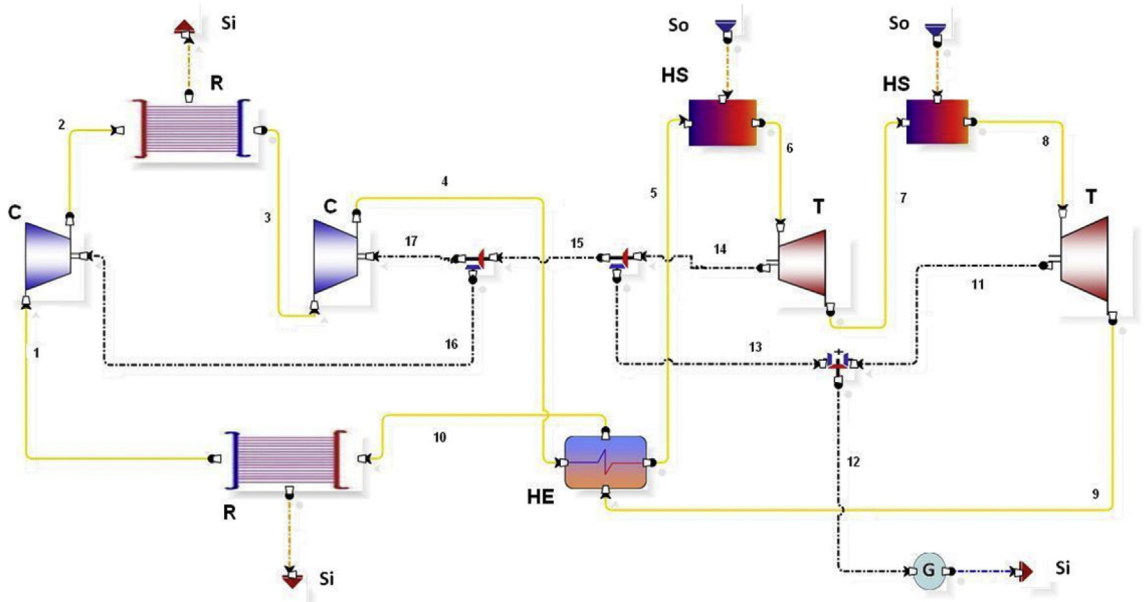

Fig. 7. Layout of the simulated regenerated-reheated-intercooled (R-R-I-B) Brayton cycle. C-Compressor; T-Turbine; HE- Heat Exchanger; R- Radiator; HS-Heat Source; G-Generator; So-Source; Si-Sink; —: *Working Fluid*; -·-·-·-·-: *Power (shaft, electric and heat.*

Please cite this article in press as: Toro C, Lior N, Analysis and comparison of solar-heat driven Stirling, Brayton and Rankine cycles for space power generation, Energy (2016), http://dx.doi.org/10.1016/j.energy.2016.11.104

Table 3
Simulations results.

Cycle parameter	Regenerative Brayton (R-B)				Regenerative Rankine (R-R)			
	CAMEL-Pro™		[12]		CAMEL-Pro™		[12]	
	H_2	N_2	H_2	N_2	Ar	N_2	Ar	N_2
p_L [bar]	1	1	1	1	0.75	0.15	0.75	0.15
T_L [K]	200	200	200	200	84	64	84	64
π	8	8	8	8	200	1000	200	1000
TIT [K]	1500	1500	1500	1500	1500	1500	1500	1500
$\eta_{I\ [\%]}$	63.72	64.15	63.22	63.39	77.87	84.25	77.88	84.61
ε [%]	63.8	64.32	63.37	63.54	78.3	84.63	78.2	84.96
ψ [kW/m^2]	0.782	0.792	0.8499	0.868	0.01413	0.00797	0.01435	0.00816

Table 4
The state properties of the computed regenerative Brayton cycles (R-B).

		R-B					
Working fluid		*N_2*			*H_2*		
State	*p*	*T*	*h*	*s*	*T*	*h*	*s*
1	101.3	200	−102	6.42	200	−1392	59.08
2	1013	422	129	6.51	424	1817	60.31
3	1013	898	648	7.33	861	8193	70.63
4	1013	1500	1370	7.94	1500	18,017	79.13
5	101.3	918	671	8.04	881	8489	80.47
6	101.3	444	152	7.25	443	2100	70.46

Table 5
The state properties of the computed regenerative Rankine cycles (R-R).

	R-R							
Working fluid	*Ar*				*N_2*			
State	*p*	*T*	*h*	*s*	*p*	*T*	*h*	*s*
1	0.75	84	−276	1.33	0.15	64	−458	2.46
2	150	90	−263	1.37	150	69	−436	2.53
3	150	177	−154	2.19	150	220	−136	4.84
4	150	1500	633	3.67	150	1500	1386	7.15
5	0.75	313	8	3.96	0.15	373	78	7.64
6	0.75	105	−101	3.39	0.15	84	−222	6.09

Table 6
The state properties of the computed regenerative – reheated Brayton cycle.

		R-R-B		
Working fluid		*N_2*		
State	*p*	*T*	*h*	*s*
1	101.3	200	−102	6.42
2	1013	422	129	6.51
3	1013	1151	945	7.62
4	1013	1500	1370	7.94
5	320.3	1171	968	7.98
6	320.3	1500	1370	8.28
7	101.3	1171	968	8.32
8	101.3	443	151	7.24

Once our model was thereby validated, we proceeded with the simulation of different more advanced plant configurations. Intercooling and reheating were added to the Brayton cycle (Figs. 4, 6 and 7) and reheat was added to the Rankine cycle (Fig. 5).

For the cycles with reheating (Figs. 4, 5 and 7) the same output temperature was assumed for both heat sources (1500 K); similarly for the intercooled cycles the outlet temperatures of the radiators was set at the same value (200 K). Both the low pressure and temperature were chosen in agreement with the assumptions of [12].

Table 7
The state properties of the computed regenerative – reheated Rankine cycle.

	R-R-R							
Working fluid	*Ar*				*N_2*			
State	*p*	*T*	*h*	*s*	*p*	*T*	*h*	*s*
1	0.75	84	−276	1.33	0.15	64	−458	2.46
2	150	90	−263	1.37	150	70	−434	2.56
3	150	344	5	2.86	150	520	230	5.91
4	150	1500	633	3.67	150	1500	1386	7.15
5	10.6	619	167	3.76	4.7	716	444	7.30
6	10.6	1500	626	4.23	4.7	1500	1372	8.17
7	172	618	167	4.32	0.15	715	443	8.33
8	0.75	105	−101	3.39	0.15	85	−221	6.10
	0.75							

Table 8
The state properties of the computed regenerative – intercooled Brayton cycle (R-I-B).

		R-I-B		
Working fluid		*N_2*		
State	*p*	*T*	*h*	*s*
1	101.3	200	−102	6.42
2	320.3	290	−8.11	6.46
3	320.3	200	−102	6.08
4	1013	290	−7.8	6.12
5	1013	898	648	7.32
6	1013	1500	1370	7.94
7	101.3	918	671	8.03
8	101.3	307	10	6.86

Table 9
The state properties of the computed regenerative – intercooled-reheated Brayton cycle (R-R-I-B).

		R-I-B		
Working fluid		*N_2*		
State	*p*	*T*	*h*	*s*
1	101.3	200	−102	6.41
2	320.3	290	−8.11	6.46
3	320.3	200	−102	6.08
4	1013	290	−7.8	6.12
5	1013	1151	945	7.62
6	1013	1500	1370	7.94
7	320.3	1171	968	7.98
8	320.3	1500	1370	8.28
9	101.3	1171	968	8.32
10	101.3	443	161	7.24

The computed values of *T*, *h* and *s* at all the cycle states are shown in Tables 4–9 for the Brayton and Rankine cycles.

Please cite this article in press as: Toro C, Lior N, Analysis and comparison of solar-heat driven Stirling, Brayton and Rankine cycles for space power generation, Energy (2016), http://dx.doi.org/10.1016/j.energy.2016.11.104

Table 10
Assumed cycle component characteristics [15].

Parameter	Value
$\eta_{pol,T}$	0.9
$\eta_{pol,C}$	0.88
η_{pump}	0.9
ΔT_{HE}	20 K

The main operational parameters of the simulated Rankine and Brayton cycles and the chosen hardware characteristics are shown in Table 10.

The Stirling engine component model implemented on CAMEL is based on the pseudo-Stirling model developed in Ref. [42] and applied also in Ref. [43]. In the Pseudo Stirling cycle the isothermal gas exchange processes of the ideal cycle are replaced, in the limit, by two isentropic processes associated with, first an isochoric undercooling and then an isochoric after heating. The Pseudo-Stirling cycle is purported to more realistically model the ideal working processes of the Stirling engine and enable optimized ideal compression ratios, for maximum thermal efficiency, to be established. The main parameters of the Pseudo Stirling cycle are the volumetric compression ratio r_v, the regenerator effectiveness ε_r, the cycle temperature ratio $\varsigma = T_{min}/T_{max}$ and the isentropic gas index $\gamma = c_p/c_v$. To access the suitability of the Pseudo-Stirling model, to validate the implemented component and calibrate cycle parameters the data given in Ref. [25] have been used as reference.

Comparison of the Stirling cycle efficiency vs cycle temperature ratio between the literature data and our model results is shown in Fig. 8, where that efficiency is evaluated as a percentage of the related Carnot efficiency. Table 11 shows the corresponding cycle parameters.

The computed values of *T*,*h*, and *s* at all the cycle states (Fig. 8) are shown in Table 12.

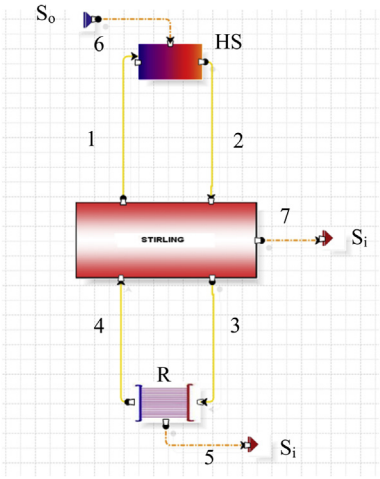

Fig. 8. Layout of the simulated Stirling Cycle (HS-Heat Source; R–Radiator; So-Source; Si-Sink). —: Working Fluid; -•-•-•-•-: Power (electric and heat).

4. Radiator analysis

As anticipated in the introduction, the radiator may be the key component of the whole system because of its size and weight, which must therefore be optimized to reduce the cost of the generated electricity.

Various radiator design concepts are available in the literature for use in space to meet specific heat rejection requirements. Fleming and co-workers [44,45] investigated heat rejection options for a closed Brayton cycle (CBC) of the Space Station Solar Dynamic Power System considering single-phase vs two-phase, and heat-pipe vs pumped-loop as major design options. Their results indicated that due to the wide range of waste heat temperatures of a CBC loop working fluid, a two phase system was not practical and for the same reason a heat pipe system is less efficient than flow through a single phase pumped-loop radiator.

Such a configuration was indeed implemented for the NASA Ground Test Demonstration [20] where the waste heat removal system consisted of two identical aluminum honeycomb radiator panels plumbed in series in a closed pumped liquid loop design. The waste heat system was integrated into the CBC loop by means of a gas to liquid heat exchanger. The coolant chosen was *n*-Heptane with FC75 as a backup coolant.

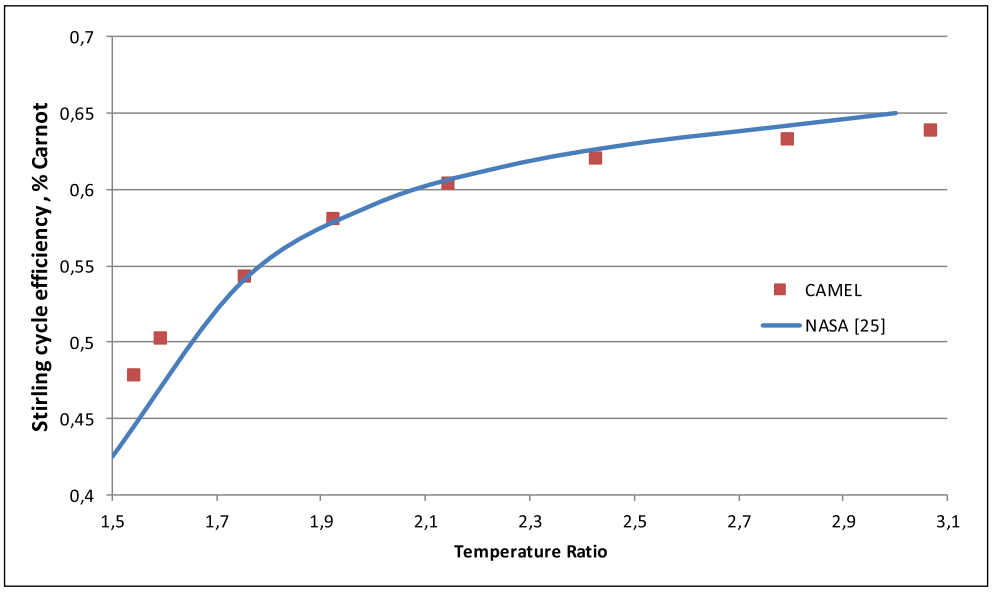

Fig. 9. Stirling cycle efficiency vs temperature ratio.

Please cite this article in press as: Toro C, Lior N, Analysis and comparison of solar-heat driven Stirling, Brayton and Rankine cycles for space power generation, Energy (2016), http://dx.doi.org/10.1016/j.energy.2016.11.104

Table 11
Assumed Stirling Engine component characteristics [25,43].

Parameter	Unit	Value
Stirling engine regenerator effectiveness ε_r	–	0.95
Stirling engine mechanical efficiency, ε_m	–	0.85
Stirling engine ΔT_{heater}	K	125
Stirling engine ΔT_{low}	K	60
Stirling engine heater effectiveness ε_h	–	0.95
Stirling engine compression ratio, r_v	–	1.7

Table 12
The state properties of the computed He, H_2 and N_2 Stirling cycles.

		He, N_2 and H_2 Stirling cycles					
Cycle working fluid		*N_2*			*H_2*		
State	*p*	*T*	*h*	*s*	*T*	*h*	*s*
1	101.3	1450	17,575	88.14	1450	1334	8.58
2	1013	1500	18,374	88.68	1500	1396	8.62
3	1013	250	−329	62.26	250	−24	6.65
4	1013	200	−1035	59.11	200	−76	6.42

A possible reduction of global radiator weight could be achieved by using "Liquid Droplet" or "Liquid Sheet" radiators [46,47], where the heat transfer fluid, often a liquid metal, is evaporated into space. As analyzed in Ref. [48], the substitution of their heat pipe radiator with a liquid droplet radiator allows a reduction of the system specific mass by 27% and of the radiator heat transfer area by 46%.This type of radiators are therefore considered by some researchers to be the most promising technology for heat rejection in space, but due to the loss of cooling liquid the related advantage of lower structure weight may be overcome by the disadvantages of having to bring up large quantities of coolant, and due to some unforeseen consequences of releasing the liquid into space in the power station vicinity. We therefore limited our analysis to traditional radiators without cooling liquid and its evaporation.

To calculate the radiator heat transfer area as a function of the cycles' parameters, working fluid and temperatures, a heat exchanger model was developed. For our model we assumed an aluminium flat-plate design with the same specification used in Ref. [15] but having a direct exchange between the working fluids and radiator without secondary fluid. Following guidance from past experience [6], a fin-tube configuration made from 0.3 mm thick aluminum sheets with a fluid flow tube diameter of 5 mm, and inter-tube spacing of 11.5 cm was adopted [15].

Due to the ambient conditions of absence of atmosphere and extremely low temperature in this application, the major contribution to the overall heat exchange between the radiator and the ambient is by radiation, but conduction and convection have major role in the heat transfer inside the working fluid conduits.

The equation for calculating the radiator heat transfer area needed to reject the heat rate Q_{rej} is:

$$A_{rad} = \frac{Q_{rej}}{U \Delta T_{lm}}, \tag{9}$$

where ΔT_{ml}, the logarithmic mean temperature difference between the hot side and cold side of the exchange in the radiator, defined as

$$\Delta T_{ml} = \frac{(T_{in,r} - T_s) - (T_{out,r} - T_s)}{\ln \frac{(T_{in,r} - T_s)}{(T_{out,r} - T_s)}}, \tag{10}$$

where T_s is the space temperature. In Eq. (9) U_{rad} is the radiator global heat exchange coefficient that could be calculated by:

$$U_{rad} = \frac{1}{\frac{t}{k} + \frac{1}{h_c} + \frac{1}{h_r}}, \tag{11}$$

where k is the thermal conductivity of the radiator plate separating the working fluid from the surrounding space, t is its thickness, and h_c represents the convective heat transfer coefficient given here by

$$h_c = \frac{0.023k}{\delta} Re^{0.8} Pr^{0.4}, \tag{12}$$

where the Reynolds number was calculated assuming a fluid velocity of 1/3 the speed of sound calculated based on fluid properties, and thus also in the turbulent flow range; while h_r is the radiative heat transfer coefficient calculated by

$$h_r = \varepsilon\sigma(\Delta T_{ml} + T_s)\left(\Delta T_{ml}^2 + T_s^2\right) \tag{13}$$

It is assumed that the surface emittance $M_e = 1$, which can be approximately attained by proper exterior surface treatment.

Table 13
Properties used in the development of h_c at the average heat rejection temperatures of the simulated Rankine, Brayton and Stirling cycles [35].

Working fluid		*Ar*	*H_2*	*N_2*
c, m/s	p = 1 bar T = 320 K	–	1361	364
	p = 0.75 bar T = 95 K		–	–
	p = 0.15 bar T = 74 K	179.38	–	174
	p = 1 bar T = 225 K	–	1145	305
ρ, kg/m³	p = 1 bar T = 320 K	–	0.0756	1.05
	p = 0.75 bar T = 95 K		–	–
	p = 0.15 bar T = 74 K	3.88	–	0.68
	p = 1 bar T = 225 K	–	0.107	1.49
Re	p = 1 bar T = 320 K	–	18,353	34,027
	p = 0.75 bar T = 95 K		–	–
	p = 0.15 bar T = 74 K	149,333	–	38,804
	p = 1 bar T = 225 K	–	28,371	53,219
Pr	p = 1 bar T = 320 K	–	0.688	0.714
	p = 0.75 bar T = 95 K	0.696	–	-
	p = 0.15 bar T = 74 K	–	–	0.804
	p = 1 bar T = 225 K	–	0.73,255	0.7375
h_c, W/m²K	p = 1 bar T = 320 K	–	1993	465
	p = 0.75 bar T = 95 K	333	–	–
	p = 0.15 bar T = 74 K	–	–	133
	p = 1 bar T = 225 K	–	2070	497

Please cite this article in press as: Toro C, Lior N, Analysis and comparison of solar-heat driven Stirling, Brayton and Rankine cycles for space power generation, Energy (2016), http://dx.doi.org/10.1016/j.energy.2016.11.104

Table 14
Radiator heat transfer resistances [m^2K/W] and global heat transfer coefficient U_{rad} [W/m^2K].

Cycle	Resistance	Working fluid		
		H_2	N_2	Ar
Rankine (R-R, R-R-R)	$R_{conductive}$	–	1 (10^{-6})	1.2 (10^{-6})
	$R_{convective}$		7.5 (10^{-3})	3 (10^{-3})
	$R_{radiative}$		48.13	22.56
	U_{rad}		2.07 (10^{-2})	4.43 (10^{-2})
Brayton (R-B,R-R-B)	$R_{conductive}$	1.4 (10^{-6})	1.4 (10^{-6})	–
	$R_{convective}$	4.9 (10^{-4})	2.1 (10^{-3})	
	$R_{radiative}$	0.714	0.62	
	U_{rad}	1.4	1.58	
Brayton (R-I-B,R-R-IB) High Pressure Radiator	$R_{conductive}$	–	1.4 (10^{-6})	–
	$R_{convective}$		8 (10^{-4})	
	$R_{radiative}$		1.27	
	U_{rad}		0.786	
Brayton (R-I-B,R-R-IB) Low Pressure Radiator	$R_{conductive}$	–	1.4 (10^{-6})	–
	$R_{convective}$		2.1 (10^{-3})	
	$R_{radiative}$		1.15	
	U_{rad}		0.863	
Stirling	$R_{conductive}$	1.4 (10^{-6})	1.4 (10^{-6})	–
	$R_{convective}$	4.78 (10^{-4})	1.98 (10^{-3})	
	$R_{radiative}$	1.61	1.6105	
	U_{rad}	0.62,073	0.6209	

TIT = 1500; $\pi = 10$ for Brayton cycles; $\pi = 1000$ for Rankine cycles with N_2; $\pi = 200$ for Rankine cycles with Ar.
(R-B Regenerative Bryton; R-R Regenerative Rankine; R-R-R Regenerative-Reheated-Rankine; R-R-B Regenerative-Reheated-Brayton; R-I-B Regenerative-Intercooled-Brayton; R-R-I-B Regenerative-Reheated-Intercooled-Brayton).

Including (11) in (8) yields

$$\Psi = \frac{U_{rad}}{[(1/\eta_I) - 1]} = \frac{1\Big/\left[\frac{t}{k} + \frac{1}{h_c} + \frac{1}{h_r}\right]}{[(1/\eta_I) - 1]} = \frac{1/[R_{cond} + R_{conv} + R_{rad}]}{[(1/\eta_I) - 1]} \tag{14}$$

From Tables 13 and 14 we can see how under the analyzed operational conditions $U_{rad} \cong \frac{1}{R_{rad}}$ and consequently

$$\Psi \approx \frac{1/[R_{rad}]}{[(1/\eta_I) - 1]} = \frac{\varepsilon\sigma(\Delta T_{ml} + T_s)\left(\Delta T_{ml}^2 + T_s^2\right)}{[(1/\eta_I) - 1]} \tag{15}$$

where the direct dependence of ψ on ΔT_{ml}, T_s, and η_I is clear.

5. Cycle analysis

Table 15 presents a performance comparison of thermal (energy) and exergy efficiencies, and power to radiator area ratio for the different types of cycles studied here.

In the case of the regenerated Brayton (R-B) the use of the working fluids, H_2, N_2 or a mixture of both, resulted in nearly the same performance, with N_2 showing a slightly higher values of all three considered parameters. We have therefore proceeded with the analysis of more complex system layouts using just N_2.

Table 16
The efficiency of the same Rankine and Brayton cycles when operating on earth.

Cycle	η_I
R-B	44%
R-R	40%
R-R-R	45%
R-R-B	47.3%
R-I-B	52%
R-R-I-B	54.2%

Brayton cycles:TIT = 1500 K, T_L = 298 K, working fluid: Air; Rankine cycles: TIT = 773 K, T_L = 303 K, working fluid: water.

Due to the higher difference between T_L and T_H (Table 3), and to a much lower backwork ratio in the regenerative Rankine cycle (R-R-R), it has a better thermal efficiency (Eq. (4)) but a much lower specific power to radiator area ratio Ψ, which is, even in the best case (using Ar), about 100 times lower than for the Brayton cycle. The use of Argon in the R-R-R allows to have a similar Ψ as when using N_2, due to its higher U_{rad} and ΔT_{ml} (affecting A_{rad}, eq. (6)), directly affected by the fact that less heat is recuperated in the regenerator since $(1-c_p/c_v)$ is greater than that of diatomic gases, which lowers the turbine exit temperature and thus also the amount of heat available for regeneration.

Table 15
Rankine and Brayton cycles results.

Cycle parameter	*R-B*			*R-R*		*R-R-R*		*R-R-B*	*R-I-B*	*R-R-I-B*
	H_2	N_2	50%$_{vol}N_2$ 50%$_{vol}H_2$	Ar	N_2	N_2	Ar	N_2	N_2	N_2
p_L [bar]	1	1	1	0.75	0.15	0.75	0.15	1	1	1
T_L [K]	200	200	200	84	64	65	85	200	200	200
π/	10	10	10	200	1000	1000	200	10	10	10
TIT	1500	1500	1500	1500	1500	1500	1500	1500	1500	1500
$\eta_{I\ [\%]}$	61.7	62.2	67	77.87	84.25	88.9	84.28	66.6	68.1	71.8
ε [%]	61.8	62.36	70.5	78.3	84.63	89.34	84.8	70.11	71.68	75.65
ψ [kW/m^2]	0.8344	0.847	1.062	0.01413	0.00797	0.0117	0.02115	1.037	0.479	0.575

R-B Regenerative Bryton; R-R Regenerative Rankine; R-R-R Regenerative-Reheated-Rankine; R-R-B Regenerative-Reheated-Brayton; R-I-B Regenerative-Intercooled-Brayton; R-R-I-B Regenerative-Reheated-Intercooled-Brayton.

Please cite this article in press as: Toro C, Lior N, Analysis and comparison of solar-heat driven Stirling, Brayton and Rankine cycles for space power generation, Energy (2016), http://dx.doi.org/10.1016/j.energy.2016.11.104

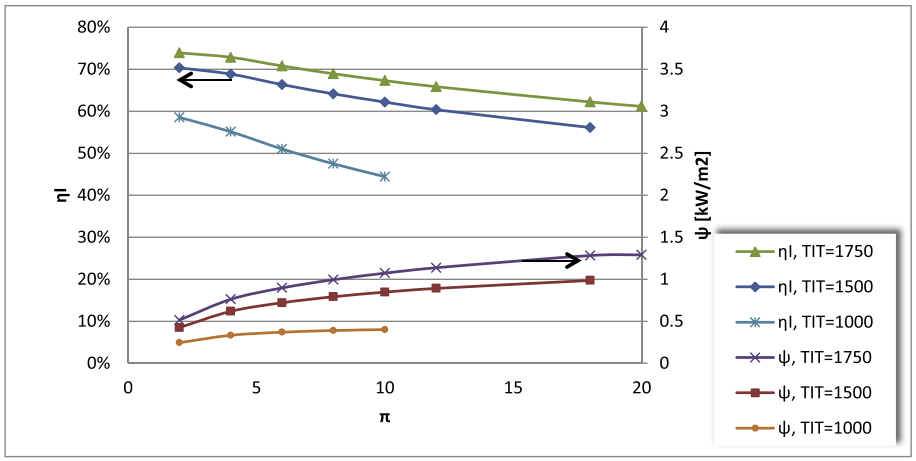

Fig. 10. Effect of π and TIT on thermal efficiency and ψ, R-B cycle (N_2).

The introduction of reheating (R-R-B) to the R-B configuration increases the thermal and exergy efficiencies by about 7% due to the increase of the regenerator inlet temperature which, through the secondary heat source, leads to better heat exchange. For a fixed flow rate this efficiency increase results in a higher outlet power and thus a higher ψ by 22% since the radiator area does not change (it keeps working between the same temperatures).

The intercooled configuration (R-I-B) shows an efficiency improvement of 9% above that of R-B while the lower radiator inlet temperature affects negatively its heat exchange efficiency causing a 50% drop in ψ.

A small improvement can be achieved by combining the intercooling with the reheating effects (R-R-I-B): a 15% improvement of efficiency and a 32% drop of the ψ value. Worse heat exchange in the radiator has a greater relative impact on ψ than on the increase of efficiency.

For comparison, the thermal efficiency of the analyzed cycles under terrestrial conditions was analyzed by using the same method, and the conditions and results are shown in Table 16, indicating the significant improvement, of 30%–40%, attainable by operation in the space environment.

Fig. 10 illustrates the trends of thermal efficiency and ψ for different TIT and π for the regenerated (R-B) Brayton cycles. For

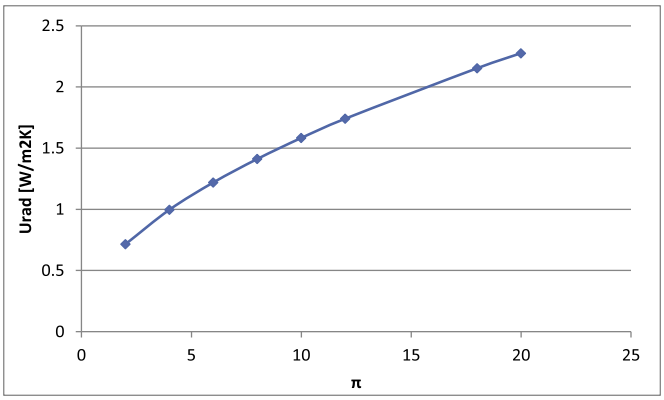

Fig. 12. Effect of pressure ratio on U_{rad}, for R-B (working fluid N_2, TIT = 1500 K).

completeness, the same parameters are shown in Fig. 10 for simple Brayton cycles where the π values are such that make regeneration impossible.

Both graphs (Figs. 10 and 11) exhibit the typical behavior of this kind of cycle. Use of a TIT of 1750 K (that at present exceeds

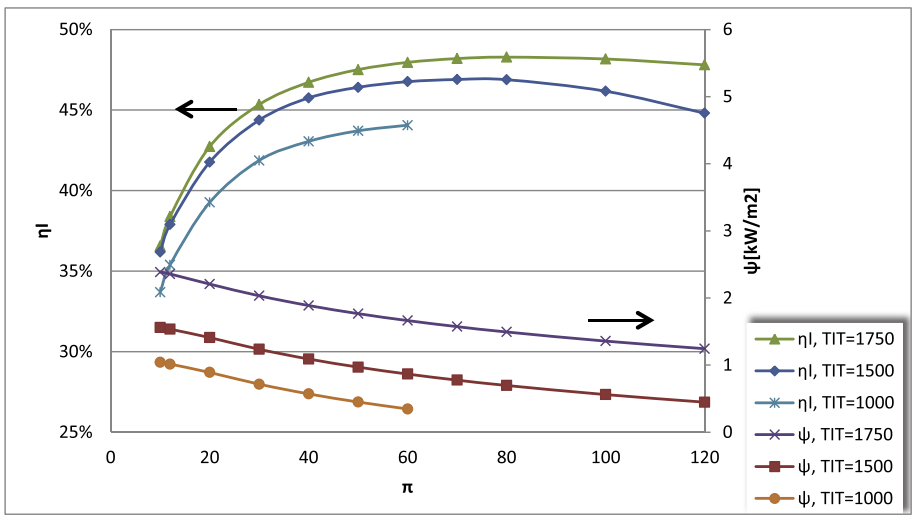

Fig. 11. Effect of pressure ratio and TIT on η_I and ψ, N_2 Brayton cycles without regenerator.

Please cite this article in press as: Toro C, Lior N, Analysis and comparison of solar-heat driven Stirling, Brayton and Rankine cycles for space power generation, Energy (2016), http://dx.doi.org/10.1016/j.energy.2016.11.104

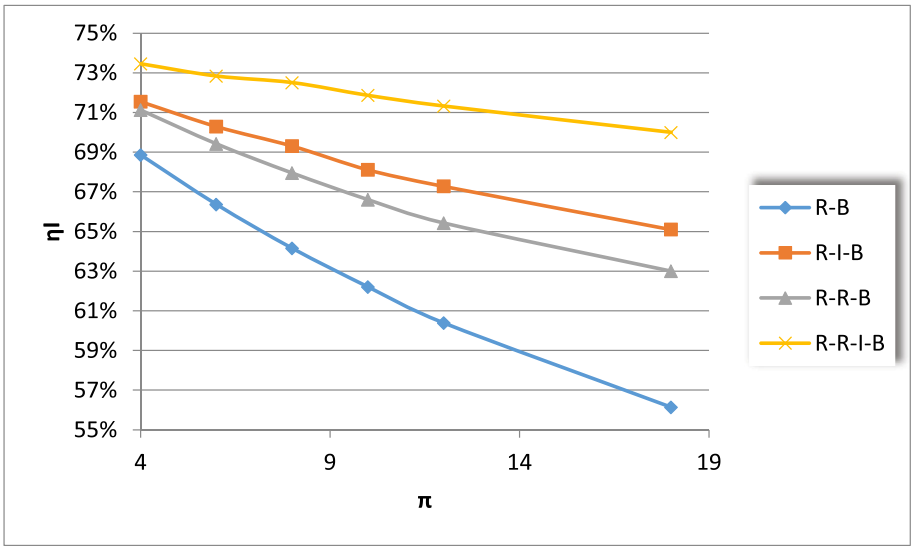

Fig. 13. Comparison of thermal efficiency of Brayton cycles with different configurations (Working fluid: N_2; TIT = 1500 K).

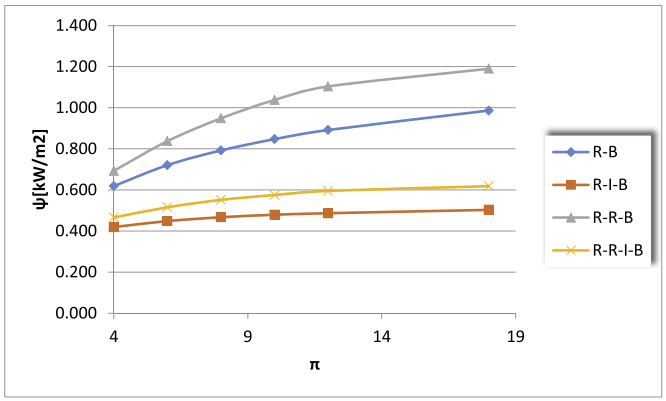

Fig. 14. Comparison of ψ of Brayton cycles with different layouts (Working fluid: N_2; TIT = 1500 K).

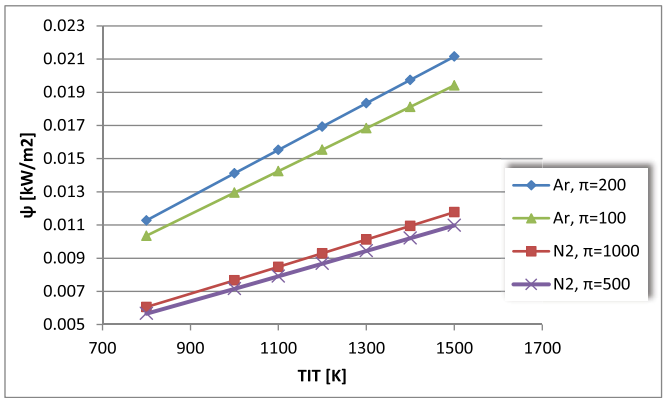

Fig. 15. Effect of π and TIT on Ψ for the R-R-R cycle.

convectional practice values but could represent future technology developments) shows that efficiencies above 70% could be reached with use of the regenerated Brayton cycle.

η_I and ψ are inversely dependent on the system pressure ratio (π) in both regenerated and not regenerated Brayton cycle for all turbine inlet temperatures.

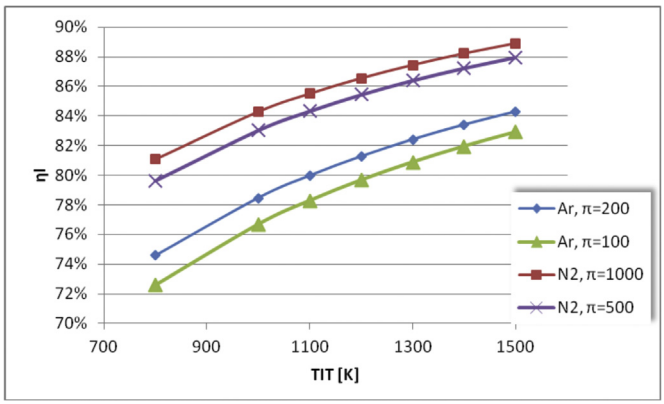

Fig. 16. Effect of π and TIT on η_I for the R-R-R cycle.

The physical explanation of such a behavior is deducible from Eq (15): the increase of π corresponds to an increase of ΔT_{ml} in the radiator and this has a stronger impact on ψ (U_{rad} is proportional to ΔT_{ml}^4) than on the decrease of η_I. As an example of that, the dependence of U_{rad} on π for the R-B cycle is shown in Fig. 12.

Figs. 13 and 14 show the effect of the cycle configuration on its thermal efficiency and ψ as a function of π. Apart from the above-described dependence of η_I and ψ on the different layouts, it is interesting to note the difference between the η_I slopes in the considered configurations.

It is in particular evident how the introduction of reheating and intercooling allows to increase the regeneration efficiency by reducing the compressor outlet temperature and increasing the turbine outlet temperature, and so diminishing the negative impact of π on the overall efficiency.

Figs. 15 and 16 show the effect of π and TIT on η_I and ψ for the R-R-R cycle. The thermal efficiency and ψ of the cycle increase significantly, as expected, with increasing TIT, while the effect of π is nearly negligible.

Table 17 presents a performance comparison of the thermal and exergy efficiency, η_I and ε, respectively, and power to radiator area ratio, ψ, for the different types of Stirling space power cycles studied here.

The results show that the efficiencies' and ψ values are the same

Please cite this article in press as: Toro C, Lior N, Analysis and comparison of solar-heat driven Stirling, Brayton and Rankine cycles for space power generation, Energy (2016), http://dx.doi.org/10.1016/j.energy.2016.11.104

Table 17
Stirling cycles results.

Cycle working fluid	H_2			N_2		
Stirling working fluid	H_2	N_2	He	H_2	N_2	He
p_L [bar]	1	1	1	1	1	1
T_L [K]	200	200	200	200	200	200
rv	2.15	2.3	1.55	2.15	2.3	1.55
T_H	1500	1500	1500	1500	1500	1500
$m_{wf,hs}$ [kg/s]	0.060	0.060	0.060	0.78	0.78	0.78
$m_{wf,cs}$ [kg/s]	0.011	0.011	0.011	0.16	0.16	0.16
$\eta_{Stirling}$ [%]	62.2	62.2	62.2	62.2	62.2	62.2
η_I [%]	52.8	52.8	52.8	52.8	52.8	52.8
ε [%]	64.8	64,8	63.3	64.8	64,8	63.3
ψ [kW/m^2]	0.483	0.483	0.483	0.483	0.483	0.483

throughout, due to the choice of optimized r_v values [42] that, once fixing the temperature ratio, reaches maximal efficiencies independently of the choice of working fluids. The use of the working fluids H_2 and N_2 in the cycle resulted in nearly the same performance and does not affect the radiator area because the contribution of the radiative exchange is much higher than the convective one (Table 11). We have therefore proceeded with the analysis considering only H_2 while H_2, N_2 as cycle working fluid and He for the Stirling engine has been included. Also for the Stirling cycle, the simulated terrestrial cycle indicate the significant improvement of 40%, attainable by operation in the space environment.

The variation of η_I and ψ with r_v and the gas index is shown in Figs. 17 and 18 for a regenerator effectiveness of 0.95 and a temperature ratio of 0.2. Only compression ratios up to 5:1 are shown since values about this figures are unrealistic for Stirling engines.

An improvement of thermal and exergy efficiency and of ψ can be reached raising the cycle higher temperature (T_H, i.e. T_2 in Fig. 9) as shown in Fig. 19. The increase of T_H/T_L has a positive effect on Stirling efficiency and thus on the cycle performance.

Stirling cycles' efficiencies are lower than those obtained by the Brayton and Rankine cycles for the same cycle T_H but with values of ψ equal to about half of those obtained by Brayton cycles but much higher than those obtained by the Rankine cycles.

It is interesting to compare Brayton and Stirling efficiencies and ψ as functions of the cycle minimal (heat sink) temperature. Fig. 20 shows the effect of T_L on Brayton and Stirling cycle efficiencies expressed as a percentage of the Carnot efficiency calculated for the same T_H and T_L. While the Brayton cycle efficiency is substantially reduced by increasing T_L, the Stirling cycle efficiency shows a small reduction, keeping it higher than 60% of the Carnot efficiency. In general, lower heat sink temperatures result in larger radiators (Fig. 21) due to the lower rejection temperatures, but smaller heat source requirement (Fig. 22). Higher heat sink temperatures lower the area of the needed radiators, but raise heat source requirement due to the lower efficiency. In the Brayton cycle the substantial

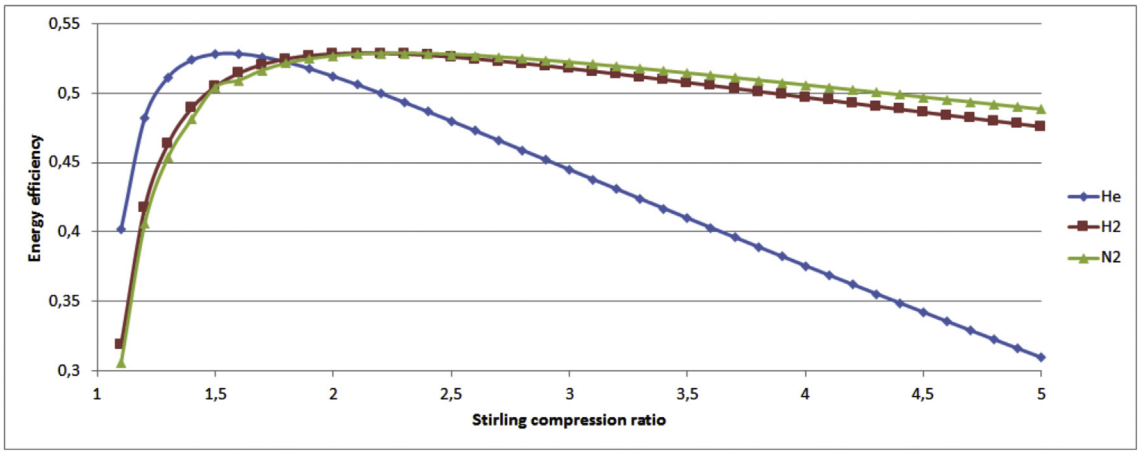

Fig. 17. Stirling cycle thermal efficiency comparison for different working fluids (T_H = 1500 K, T_L = 200 K,ε_r = 0.85).

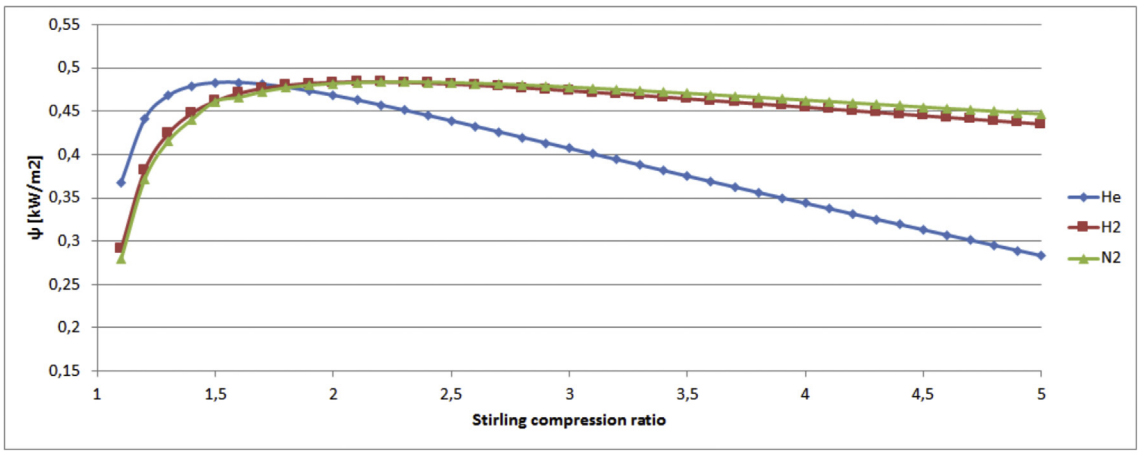

Fig. 18. Stirling cycle ψ comparison for different working fluids (T_H = 1500 K, T_L = 200 K, ε_r = 0.85).

Please cite this article in press as: Toro C, Lior N, Analysis and comparison of solar-heat driven Stirling, Brayton and Rankine cycles for space power generation, Energy (2016), http://dx.doi.org/10.1016/j.energy.2016.11.104

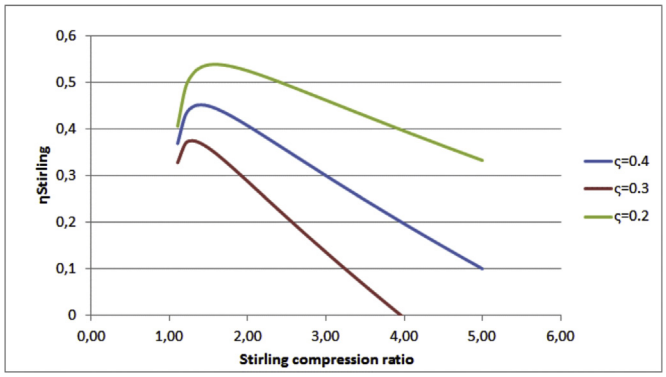

Fig. 19. Effect of compression ratio on Stirling cycle thermal efficiency (Helium; $\varepsilon_r = 0.95$).

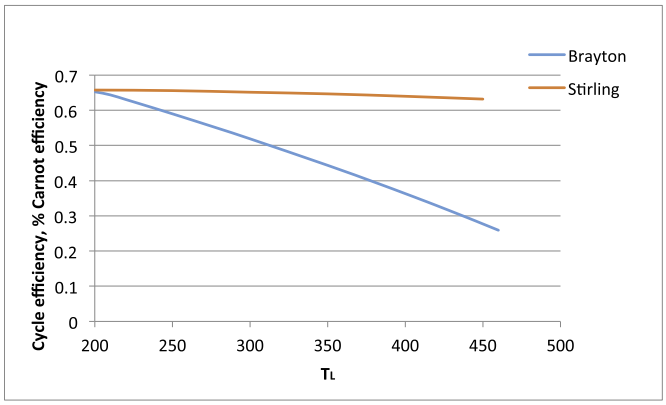

Fig. 20. Brayton (R-B, $\pi = 10$, $T_H = 1500$ K, P = 400 kW) and Stirling (Helium,$T_H = 1{,}500$ K, rv = 1.55, P = 400 kW) cycles' efficiency vs T_L.

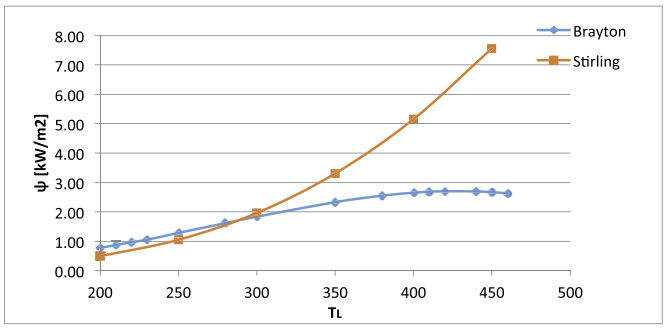

Fig. 21. Brayton (R-B, $\pi = 10$, $DT_{AHR} = 50$, $T_H = 1500$ K, P = 400 kW) and Stirling (Helium,$T_H = 1500$ K, rv = 1.55 P = 400 kW) ψ vs T_L.

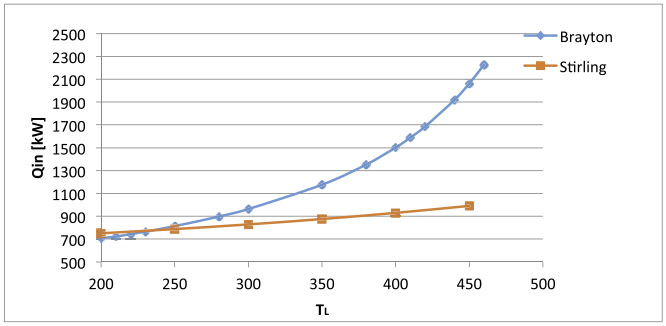

Fig. 22. Brayton (R-B, $\pi = 10$, $DT_{AHR} = 50$, $T_H = 1500$ K, P = 400 kW) and Stirling (Helium,$T_H = 1500$ K, rv = 1.55 P = 400 kW) inlet heat vs T_L.

reduction of the efficiency causes a small increase of ψ, which remain constant for T_L higher than 400 K, while for the Stirling cycle ψ increases strongly, reaching 2 kW/m^2 for a T_L of 300 K. On the hot side, the Brayton cycle shows a strong increase of the required heat from the collectors (from 700 to about 2300 kW) while in the Stirling cycle it increase from 750 to 990 kW.

6. Conclusions

Starting from past results (by the second author and his co-workers) that show the potential high efficiency of the use of terrestrial thermal cycles for power generation in space, a performance comparisons of different and more advanced Brayton, Rankine and Stirling configurations was carried out.

Under the current model assumptions, the Rankine regenerated-reheated cycle operating with N_2 showed the highest thermal efficiency of about 88.9%, while the highest efficiency for the Brayton cycle, achieved with the regenerated-intercooled-reheated configuration, was 71.8%. The analysis of the free piston Stirling cycle showed that its thermal and exergy efficiencies are lower than those obtained by the Brayton and Rankine cycles for the same cycle temperatures. The other relevant parameter considered is the power–to-radiator heat transfer area ratio ψ, which had its peak values for regenerated Brayton systems, decreased with the Brayton system complexity, and was 100-foldlower for the Rankine cycles with the considered working fluid, the latter primarily because of the lower radiator temperature necessary for condensation for the selected working fluids. The results obtained for the Stirling cycle shows that the cycle became advantageous in both efficiency and ψ increasing the cycle lower temperature.

The conflict between high efficiency and associated required high radiator area can be resolved by thermoeconomic analysis and optimization, which then could point to the best cycle to use.

Nomenclature

A	radiator area, m^2
c	speed of sound, m/s
c_p	constant pressure specific heat, kJ/(kg K)
c_v	constant volume specific heat, kJ/(kg K)
Ex	exergy rate, kW
ex	specific exergy, kJ/kg
h	enthalpy, kJ/kg
h_c	convective heat transfer coefficient, W/(m^2 K)
h_r	radiative heat transfer coefficient, W/(m^2 K)
k	thermal conductivity, W/mK
p	pressure, bar
R	Thermal resistance, (m^2 K)/W
rv	Stirling compression ratio
s	entropy, kJ/kgK
t	thickness, m
T	temperature, K
TIT	turbine inlet temperature, K
Q	heat flow, kW
U	global heat transfer coefficient, W/(m^{2}K)
W	power, kW

Greek symbols

δ	radiator equivalent diameter, m
ε	exergy efficiency
η_I	thermal efficiency
ρ	density, kg/m^3
π	pressure ratio
ψ	power produced per unit radiator area, kW/m^2
ς	Stirling cycle temperature ratio

Please cite this article in press as: Toro C, Lior N, Analysis and comparison of solar-heat driven Stirling, Brayton and Rankine cycles for space power generation, Energy (2016), http://dx.doi.org/10.1016/j.energy.2016.11.104

References

[1] Mankins J. Space solar power: a major new energy option? J Aerosp Eng 2001;14:38–45.
[2] Lior N. Power from space. Energy Convers Manag 2001;42:1769–805.
[3] Klann JL. Steady-state analysis of a Brayton space-power system. National Aeronautics and Space Administration, Lewis Research Center; 1970.
[4] Mason LS. A solar dynamic power option for space solar power. Cleveland, Ohio: Glenn Research Center; 1999.
[5] Dhar M. Stirling space engine program, Vols. 1 & 2; 1997. Final Report.
[6] Lior N. The ECOS 2009 World Energy Panel: an introduction to the Panel and to the present (2009) situation in sustainable energy development. Energy 2011;36:3620–8.
[7] Glaser PE. Power from the sun: its future. Science 1968;162:857–61.
[8] Glaser PE. An overview of the solar power satellite option. IEEE Trans Microw Theory Tech 1992;40:1230–8.
[9] Criswell DR, Thompson RG. Wireless power transmission data envelopment analysis of space and terrestrially-based large scale commercial power systems for earth: a prototype analysis of their relative economic advantages. Sol Energy 1996;56:119–31.
[10] Brown WC. Wireless power transmission the history of wireless power transmission. Sol Energy 1996;56:3–21.
[11] Woodcock GR. Solar satellites – space key to our power future. Astronaut Aeronaut 1977;15:30–43.
[12] Tarlecki J, Lior N, Zhang N. Analysis of thermal cycles and working fluids for power generation in space. Energy Convers Manag 2007;48:2864–78.
[13] Zidanšek A, Ambrožič M, Milfelner M, Blinc R, Lior N. Solar orbital power: sustainability analysis. Energy 2011;36:1986–95.
[14] Wu Y-T, Ren J-X, Guo Z-Y, Liang X-G. Optimal analysis of a space solar dynamic power system. Sol Energy 2003;74:205–15.
[15] S.o.S.D.P.S. Branch. In: O. Lewis Research Center Cleveland, editor. Solar dynamic power system development for space station freedom; 1993.
[16] Tsujikawa Y. Optimum heat rejection in Brayton cycle solar dynamic power system. Clean and Safe energy forever. Proc Int Sol Energy Soc Kobe City, Jpn 1990;1989(2):1358–62.
[17] Glassman A, Stewart W. A look at the thermodynamic characteristics of Brayton cycles for space power Summer Meeting. American Institute of Aeronautics and Astronautics; 1963.
[18] Mackay DB. Powerplant heat cycles for space vehicles. Inst Aero Sci; 1959.
[19] Davis JE. Design and fabrication of the Brayton rotating unit. Lewis Research Center, NASA; 1972.
[20] Mason LS, Kudija CT. Solar dynamic ground test demonstration (SD GTD) system test plans. Joint Solar Engineering Conference. ASME; 1994.
[21] Shaltens RK, Mason LS. 800 Hours of operational experience from a 2kWe solar dynamic system. Cleveland, Ohio: NASA Lewis Research Center; 1999.
[22] Mason LS, Schreiber JG. A historical review of Brayton and Stirling power conversion technologies for space applications space nuclear conference. 2007.
[23] Agazzani A, Massardo A. Advanced solar dynamic space power systems, Part I: efficiency and surface optimization. J Sol Energy Eng 1995;117:265–73.
[24] Agazzani A, Massardo A. Advanced solar dynamic space power systems, Part II: detailed design and specific parameters optimization. J Sol Energy Eng 1995;117:274–81.
[25] Slaby JG. Overview of free-piston stirling engine technology for space power application. In: Solar energy conference, Honolulu, Hawaii, USA; 1987.
[26] Mason LS. A comparison of fission power system options for lunar and mars surface applications. In: Space technology and applications international forum (STAIF–2006), Albuquerque, New Mexico, USA; 2006.
[27] Dhar M. Stirling space power program, Vols. 1 & 2; 1997. Final Report.
[28] Wood JG, Neill L. Advanced 35 W free-piston stirling engine for space power applications. In: Space technology and applications international forum–STAIF 2003; 2003.
[29] Toro C, Lior N. Analysis and comparison of different thermal cycles for power generation in space. In: Proceedings of the 27th international conference on efficiency, cost, optimization, simulation and environmental impact of energy systems, ECOS 2014; 2014.
[30] Amati V, Coccia A, Sciubba E, Toro C. CAMEL-pro users manual, rev, vol. 4; 2010. www.turbomachinery.it.
[31] Università di Roma. La Sapienza. CAMEL-pro users manual, v.4. 2008. www.turbomachinery.it.
[32] Amati V, Sciubba E, Toro C. Exergy analysis of a solid oxide fuel cell-gas turbine hybrid power plant. 2009. p. 721–31.
[33] Sciubba E, Toro C. Modeling and simulation of a hybrid PV/thermal collector. In: ECOS 2011, Novi Sad, Serbia; 2011.
[34] Colonna P, van der Stelt T. FluidProp: a program for the estimation of thermo physical properties of fluids. The Netherlands: Energy Technology Section, Delft University of Technology; 2004. http://wwwFluidPropcom.
[35] Lemmon EW, Huber ML, McLinden MO. NIST standard reference database 23: reference fluid thermodynamic and transport properties-REFPROP, Version 9.1. 2013.
[36] Shaltens RK, Mason LS. Early results from solar dynamic space power system testing. J Propuls Power 1996;12:852–8.
[37] Martini WR. Stirling engine design manual. 1983.
[38] Clarke RG, Taylor DR. Experiences in the commissioning of a prototype 20kW helium charged Stirling engine. In: Seventeenth intersociety energy conversion engineering conference; 1982. p. 1796–800.
[39] Walker G. Stirling cycle machines. Oxford: Clarendon Press; 1973.
[40] Yamamoto T, Furuhata T, Arai N, Lior N. Analysis of a high-efficiency low-emissions "chemical gas turbine" system. J Propuls Power 2002;18:432–9.
[41] Ulizar I, Pilidis P. Design of a semiclosed-cycle gas turbine with carbon dioxide–argon as working fluid. J Eng Gas Turbines Power 1998;120:330–5.
[42] Reader GT. The pseudo stirling cycle – a suitable performance criterion. In: 13th Intersociety Energy Conversion Engineering Conference, San Diego; 1978. p. 1763–70.
[43] Rokni M. Thermodynamic analysis of SOFC (solid oxide fuel cell)–Stirling hybrid plants using alternative fuels. Energy 2013;61:87–97.
[44] Fleming M, Hoehn F. Radiator selection for space station solar dynamic power systems. Energy – New Front 1987;1:208–13.
[45] Fleming M, Flores RR. Solar dynamic radiator design development. In: Joint solar engineering conference ASME 1994, San Francisco, California; 1994.
[46] Tagliafico LA, Fossa M. Lightweight radiator optimization for heat rejection in space. Heat Mass Transf 1997;32:239–44.
[47] Mattick AT, Hertzberg A. Liquid droplet radiators for heat rejection in space. J Energy 1981;5:387–93.
[48] Massardo AF, Tagliafico LA, Fossa M, Agazzani A. Solar space power system optimization with ultralight radiator. J Propuls Power 1997;13:560–4.

Please cite this article in press as: Toro C, Lior N, Analysis and comparison of solar-heat driven Stirling, Brayton and Rankine cycles for space power generation, Energy (2016), http://dx.doi.org/10.1016/j.energy.2016.11.104